Contact Angle of Air Bubbles Attached to an Air-Water Surface in Foam Applications

L. A. Lobo, A. D. Nikolov,† A. S. Dimitrov,† P. A. Kralchevsky,† and D. T. Wasan*

Department of Chemical Engineering, Illinois Institute of Technology, Chicago, Illinois 60616

Received March 27, 1989. In Final Form: December 20, 1989

A new method is developed to measure the contact angle of air bubbles attached to an air-water interface. The measurements made from the microscopic interference pattern (Newton rings), which are obtained by viewing the bubble in reflected light, are used in conjunction with the solutions of the Laplace equations to the fluid interfaces to obtain the contact angle of the film. Measurements made from a differential microscopic interference pattern were used to check the validity of the results.

Introduction

The interactions between fluid surfaces are an important factor in the stability of dispersed systems. One way to study these interactions involves measuring the contact angle of thin fluid films formed by fluid droplets attached to fluid interfaces. From the contact angle we can obtain the film tension, which is directly related to the change in the free energy of the film. These films can be likened to the films that exist in real dispersed systems.

In the literature, several different methods have been proposed to measure the contact angle between the film and the meniscus of a fluid-fluid system. Huisman and Mysels[1,2] have developed the method for a gas bubble lying over a liquid. To determine the contact angle, they extrapolated the interfaces from photomicrographs of the elevation of the bubbles. Light interference methods, on the other hand, have a definite advantage over the photomicrographic method in relation to their reliability and accuracy. This is because interference fringes represent a vertical distance, between surfaces, which is smaller than the resolution obtained from photomicrographs of elevations of the surfaces. Princen[3,4] and DeFeijter et al.[5] used a laser diffraction pattern to obtain the meniscus profile and contact angle for plane verticle films using geometrical equations for the meniscus profile. Scheludko et al.,[6,7] in studies of planar films, developed the "topographic" method, where the approximate meniscus profile and hence the contact angle are derived from the radii of the interference rings surrounding the film perimeter. However, the value of the capillary pressure of planar films is limited by the size of the capillary used. In real systems, the actual capillary pressures that exist in foams can be approximated by the height of stable foams and can have a magnitude of up to 1000-1500 Pa. It is known that the film contact angle can be a function of the capillary pressure, especially at higher values of the pressure.[8] The contact angle at high capillary pressures could be determined by studying small fluid droplets (diameter less than 400 μm) attached to a fluid interface. In this study, we propose a method to calculate the contact angle of aqueous films, formed by floating air bubbles, from their microscopic interference pattern. We used the air-water system because of its applications to foams. The experimental method we used was similar to the "shrinking bubble" method used by Princen and Mason.[9] In this method, a relatively large bubble at a liquid surface gradually decreases in size due to the gas escaping from within the bubble to the atmosphere, through the permeable liquid film. The geometric parameters of the bubble are recorded optically as a function of its size. Ivanov and co-workers[10-13] also used the same experimental technique to study the effect of film and line tension, in the case of small bubbles. By measuring the equatorial diameter and the radius of contact of the film, they calculated the contact angle using the asymptotic solutions of the Laplace equation that describes the surface of the bubble. Determining the contact angle for their system (sodium dodecyl sulfate with electrolyte) was simplified by the fact that the surfactant film was thin and the radius of contact could be measured precisely. In the case of systems with small contact angles (<4°), the radius of contact is not visually distinct and cannot be accurately measured. In this case, while viewing the bubble from the top in reflected light, we observe an interference pattern (Newton rings), in the three-phase contact region. Our new method utilizes the radii of the Newton rings to determine the contact angle, without using any major approximations. The Laplace equations for the surfaces were integrated numerically by using the Runge-Kutta method to obtain the profiles of the surfaces. These profiles were used to generate a set of theoretical Newton rings. To fit the experimental and theoretical radii of the Newton rings, we

* Author to whom all correspondence should be addressed.

† Present address: Laboratory of Thermodynamics and Physicochemical Hydrodynamics, Faculty of Chemistry, University of Sofia, 1126 Sofia, Bulgaria.

(1) Huisman, F.; Mysels, K. J. *J. Phys. Chem.* **1969**, *73*, 489.
(2) Mysels, K. J.; Huisman, F.; Razouk, R. *J. Phys. Chem.* **1966**, *70*, 1339.
(3) Princen, H. M.; Frankel, S. *J. Phys. Chem.* **1970**, *74*, 12, 2580.
(4) Princen, H. M.; Frankel, S. *J. Colloid Interface Sci.* **1971**, *35*, 3, 386.
(5) De Feijter, J. A.; Vrij, A. *J. Colloid Interface Sci.* **1978**, *64*, 2, 269.
(6) Scheludko, A.; Radoev, B.; Kolarov, T. *Trans. Faraday Soc.* **1968**, *64*, 2864.
(7) Kolarov, T.; Scheludko, A.; Exerowa, D. *Trans. Faraday Soc.* **1968**, *64*, 2213.
(8) Toshev, B. V.; Platikanov, D.; Scheludko, A. *Langmuir* **1988**, *4*, 489, 1988.
(9) Princen, H. M.; Mason, S. G. *J. Colloid Interface Sci.* **1965**, *20*, 353.
(10) Ivanov, I. B.; Kralchevsky, P. A.; Nikolov, A. D. *J. Colloid Interface Sci.* **1986**, *112*, 97.
(11) Kralchevsky, P. A.; Ivanov, I. B.; Nikolov, A. D. *J. Colloid Interface Sci.* **1986**, *112*, 108.
(12) Nikolov, A. D.; Kralchevsky, P. A.; Ivanov, I. B. *J. Colloid Interface Sci.* **1986**, *112*, 122.
(13) Kralchevsky, P. A.; Nikolov, A. D.; Ivanov, I. B. *J. Colloid Interface Sci.* **1986**, *112*, 132.

0743-7463/90/2406-0995$02.50/0

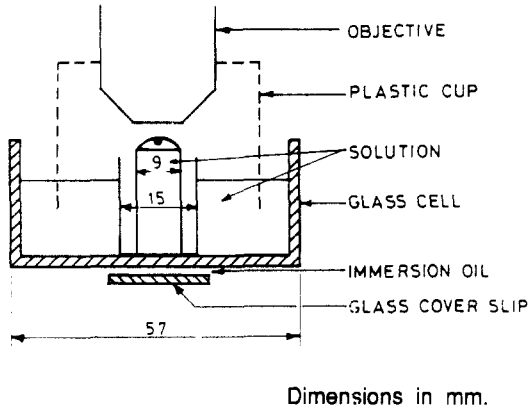

Figure 1. Schematic of the experimental cell.

adapted the general minimization procedure, (developed by Dimitrov et al.[14] for planar films) using the radius of contact r_c as the variable parameter. We verified the results obtained by this method using independent data provided by the differential interference technique proposed by Nikolov et al.[12] We also looked into the effect of micellar concentrations on the value of the contact angle. The new method that we developed can be used mainly for systems with low contact angles and thick films, the typical situation for emulsion and pseudoemulsion films[15] (aqueous films formed by oil drops attached to an air–water interface). Films (foam and emulsion) from micellar solutions exhibit stratification,[16] and the final thickness of the film (after drainage) can be large with a small contact angle, which can be measured by using this method. Change in the interactions between the micelles, either by adding electrolyte[17] (for anionic micelles) or by solubilizing oils[18] (in the case of nonionic micelles), directly affects the properties and the contact angle of the film. The contact angle measured by use of this technique will be useful in quantifying the change in the film properties due to the change in the micellar interactions.

Experimental Section

We used a Carl Zeiss Jena Epival Interphako microscope to make the contact angle measurements. This microscope is capable of viewing objects in transmitted as well as in reflected light. The light source for the reflected light mode is a mercury vapor lamp (HBO 50) used along with a multiple grating. The microscope is equipped with a Max Zhender interferometer, which splits the original beam of the image into two beams of different optical paths which when recombined give a shearing type differential interference pattern.[19] This pattern can be used to determine the curvature of surfaces. By changing the grating constant and the magnification, a range of curvatures can be measured. A specially designed glass cell held the solution in which the bubbles were created. The construction of the cell is shown in Figure 1. It consists of three concentric glass cylinders with diameters of 57, 15, and 9 mm. The cylinders were fixed on one end to an optical glass plate. Prior to use, the glass cell and all other glassware were cleaned with distilled water after soaking in freshly prepared chromic acid for 24 h. The cell was then rinsed 3 times with small quantities of the test solution. The inner cylinder was completely filled with the solution, and the outer cylinder was filled to about half its height. The middle cylinder collected the overflow from the inner cylinder. The meniscus of the solution within the inner cylinder was made almost flat by scraping the top of the cylinder with the side of a glass capillary tube. We created bubbles on the meniscus of the inner solution using a 1-mL glass syringe with a long glass tube at its tip. The bubble was created by sucking the solution within the syringe, leaving a small air gap in the glass tube; the size of the air gap determined the size of the bubbles. The solution was then expelled from the syringe. At the moment when the air pocket reached the tip of the glass tube, it formed a bubble which was deposited on top of the meniscus. The initial bubble size (diameter) was controllable to about 100 μm. A plastic cylindrical cup with a diameter between that of the outer and middle cylinders was inverted over the cell such that its edge lay below the surface of the solution in the outer cylinder. The objective fit snugly into a hole cut in the roof of the cup, such that the cup moved with the objective. The environment around the bubble was thus isolated from the outside, preventing evaporation or mechanical disturbances in the outer solution from reaching the inner solution. The microscope was mounted on a 4000-kg antivibrational block. The light sources for the transmitted and reflected light were fitted with a filter for green light (546 nm). For our measurements with reflected light, we used a multiple grating with a slit width of 48 μm. The experiments were carried out by using Shell's ethoxylated alcohol surfactant Enordet C1415 AE9 with an average of nine ethoxy groups and a 14–15 carbon atom chain. The critical micelle concentration of the solution is around 5×10^{-6} mol/L. The two concentrations studied were (i) 4 wt % (2.6×10^{-2} mol/L) of surfactant dissolved in distilled water and (ii) 1 wt % (6.6×10^{-3} mol/L) of surfactant dissolved in a 1 wt % brine solution. The brine was prepared with NaCl, obtained from Fisher Scientific, which was ACS certified. The surface tension of both solutions was 29.7 dyn/cm.

The shrinking bubble measurements were made with a single bubble at a time. The initial radii of the bubbles were about 350–375 μm. After formation of the bubbles, we waited for a period of 30 min (or longer) before taking measurements to permit saturation of the environment above the solution. All measurements were made by using an objective with a magnification of 12.5. Photomicrographs in reflected light were taken of the common and differential interference patterns as a function of time. The entire procedure took about 3 h for each bubble studied. The distance between the interference fringes was measured from the photomicrographs with a Carl Zeiss Jena moving stage micrometer (called Comparator type AB) with a magnification of 10, which has a minimum resolution of 0.2 μm. Photomicrographic as well as visual measurements were made in transmitted light in order to obtain the equatorial diameter of the bubbles. Measurements were made at suitable time intervals until the bubble shrunk to about 80 μm.

Experimental Measurements and Calculation Procedure

The main parameters required to characterize the system are (i) the radius of the bubble, R; (ii) the radius of the hat of the bubble, R_f; and (iii) the contact angle α along with the radius of contact of the film r_c (see Figure 2). The contact angle α defined in Figure 2 is twice the contact angle defined for symmetrical planar films.[4]

Measurements and Interpolation of the Equatorial Radius of the Bubble (R). The equatorial radius of the bubble can be determined by observing the bubble in transmitted light. The actual radius of the bubble, however, must be determined from the Fraunhofer diffraction pattern which appears around the bubble equator. The theoretical solution for Fraunhofer diffraction produced by an edge[20] shows that the inner edge of the

(14) Dimitrov, A. S.; Kralchevsky, P. A.; Nikolov, A. D. *Colloid Surf.*, submitted.
(15) Wasan, D. T.; Nikolov, A. D.; Huang, D. D. W.; Edwards, D. A. In *Surfactant Based Mobility Control*; Smith, D. H., Ed.; American Chemical Society: Washington, DC, 1988; p 136.
(16) Nikolov, A. D.; Wasan, D. T.; Kralchevsky, P. A.; Ivanov, I. B. In *Ordering and Organization in Ionic Solutions*; Ise, N., Sogami, I., Eds.; World Scientific: London, 1988.
(17) Nikolov, A. D.; Wasan, D. T. *J. Colloid Interface Sci.*, in press.
(18) Lobo, L. A.; Nikolov, A. D.; Wasan, D. T. *J. Dispersion Sci. Technol.* **1989**, *10*, 2, 143.
(19) Beyer, H. *Jenaer Rundsch.* **1971**, *16*, 82.
(20) Landau, L. D.; Lifschitz, E. M. In *Theoretical Physics* (in Russian); Nauka: Moscow, 1973; Vol. 2, p 191.

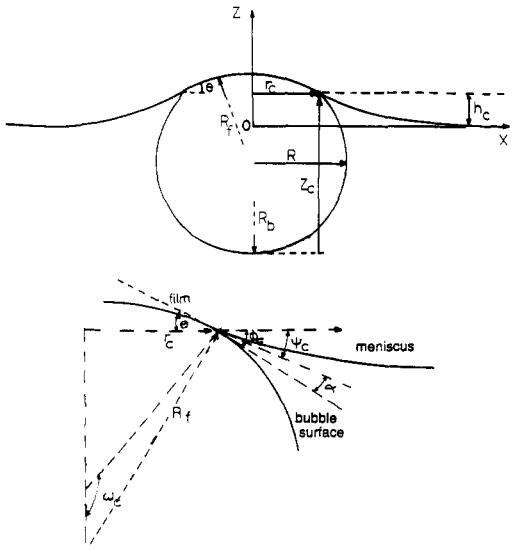

Figure 2. (a, Top) Fluid particle at a fluid–fluid interface. (b, Bottom) Definition of the angles at the three-phase contact line.

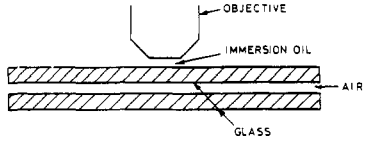

Figure 3. Experiment to measure the radius of a capillary from the Fraunhofer diffraction pattern.

first bright diffraction fringe lies close to the edge of the object. Since our light source was not ideal (the incident rays were not made parallel), we checked the solution experimentally by simultaneously observing a glass capillary of known inner diameter in reflected and transmitted light (see Figure 3). In this way, we could see that the inner edge of the first bright diffraction fringe (seen in transmitted light) was very close to the actual inner edge of the capillary (seen distinctly in reflected light). The estimated error in measuring the diameter of the bubble by using this criterion is about 0.5 μm, which is close to the resolution of the microscope.

For the calculations using common interference (CI) and differential interference (DI) measurements, we needed the values of the radius of the bubble R at the moments when the CI and DI patterns were photographed. Since it is not possible to make simultaneous measurements, suitable interpolated values of R were required at any time t. Using the method suggested by Kralchevsky et al.,[13] we found these values using the expression

$$R(t) = a_1(t_0 - t)^q + a_2(t_0 - t)t \qquad (1)$$

where a_1, a_2, t_0, and q are parameters to be determined by a least-squares fit of the experimental data. The curves obtained for single bubbles for the two surfactant solutions are shown in Figure 4. We obtained a good fit with this method with a maximum standard deviation of 0.25 μm.

Measurement of Curvature of the Hat (R_f). The radius of curvature of the hat R is measured from the differential interference (DI) pattern (see Figure 5). The position of the streaks is measured, and R_f is given by[12]

$$R_f = [(1 + d^2/l_k^2)(x_k^2 + l_k^2/4)]^{1/2} \qquad (2)$$

where $l_k = k\lambda/4$, k is the order of interference of a streak (k = 1, 2, 3, ...) λ is the wavelength of incident light (in μm), d is the distance of shearing of the image (in μm),

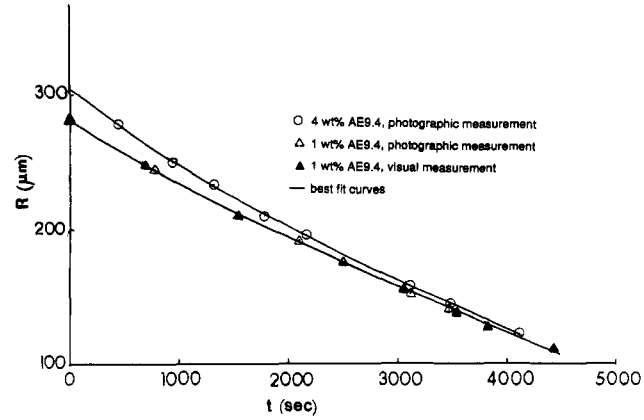

Figure 4. Equatorial radii of the bubbles as a function of time.

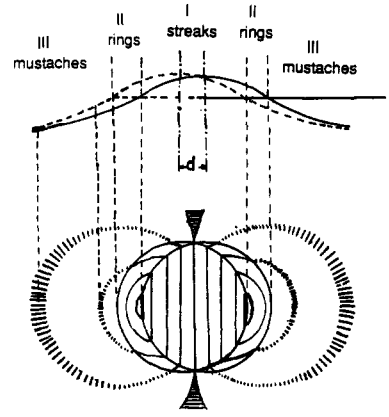

Figure 5. Cross section of the reflecting surfaces sheared horizontally by a distance d and the resulting differential interference pattern.

and x is the distance of the streak (in μm) from the central streak (position of zero order of interference).

Since it is extremely difficult to determine the exact position of the central coordinate, we used the procedure developed by Nikolov et al.[12] A function Φ is defined

$$\Phi(a') = \sum_n [R_f(x'_{l,n} - a') - R_f(x'_{r,n} - a')]^2 \qquad (3)$$

where x'_l and x'_r denote the coordinates of the left and right of pairs of symmetric streaks numbering n away from an arbitrarily chosen origin for the central axis. The value of R_f is calculated from eq 2. The value $\bar{a}$ of a' which minimizes $\Phi(a')$ is the most probable value of the central axis, and the coordinates of the streaks are given by

$$x_n = x'_n - \bar{a} \qquad (4)$$

Calculation of Contact Angle α Using Common Interference (CI). In this subsection, we propose a method to calculate the contact angle α using measurements of the radii of the common interference rings. When the films are thick (>200 Å), the radius of contact r_c cannot be accurately measured, and we use the Newton rings and equatorial radius R to determine r_c as well as the contact angle α. The calculation procedure consists of the following steps.

i. Calculation of the Radius of Curvature of the Bottom of the Bubble (R_b). Due to the buoyancy of the air bubble, its lower surface is flattened or deformed. The radius of curvature at the bottom of the bubble can be calculated from the measured equatorial radius by using an expression suggested by Kralchevsky et al. (see eq 15

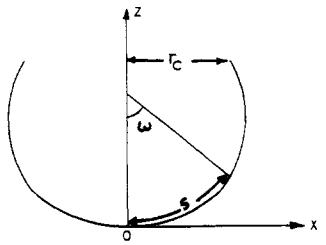

Figure 6. Sketch of the bubble surface with the coordinate axes used for the integration of the Laplace equation from the boundary $z = 0$, $x = 0$, $\omega = 0$ to $x = r_c$.

in ref 11)

$$\frac{R}{R_b} = 1 - \frac{\beta}{6} + \frac{\beta^2}{6}\left(\ln 2 - \frac{1}{6}\right) + ... \qquad (5)$$

where $\beta = \Delta\rho g R_b^2/\sigma$, $\Delta\rho$ is the difference in the density of the two fluids (the solution and the air), and σ is the surface tension. Equation 5 is an asymptotic equation, and an error analysis has been performed by Kralchevsky et al.[11] For the size of bubbles we studied, the error obtained by using eq 5 is much smaller than the precision of the experimental measurements of R. Equation 5 can be solved for R_b for each given value of R by successive approximations.

ii. Shape of the Bubble Surface. The lower surface of the bubble is deformed by gravity, and in this case the Laplace equation has no closed analytical solution. We accordingly integrated this equation numerically. For the bubble surface (see Figure 6), the Laplace equation can be written in the parametric form suggested by Hartland and Hartley[21]

$$\frac{d\hat{z}}{ds} = \sin\omega \qquad \frac{d\hat{x}}{ds} = \cos\omega$$

$$\frac{d\omega}{ds} = 2 + \beta\hat{z} - \frac{\sin\omega}{\hat{x}} \qquad (6)$$

where $\hat{x}$ and $\hat{z}$ are dimensionless variables

$$\hat{x} = X/R_b \qquad \hat{z} = Z/R_b \qquad (7)$$

X and Z are the real dimensioned variables, and s is the arc length of the generatrix of the bubble surface ($ds^2 = dX^2 + dZ^2$).

An initial value for the radius of contact r_c is approximated from the measurements. The equations are integrated numercially by using the Runge–Kutta method from the coordinates $\hat{x} = 0$, $\omega = 0$, and $\hat{z} = 0$ (which is the apex of the bubble), with appropriate increments in s up to the point $X = r_c$, $\omega > 90$ (see Figure 6).

iii. Calculation of the Deformation of the Meniscus Represented by the Angle Ψ_c. At the point of contact, the tangent to the bubble surface makes an angle ϕ_c with the horizontal (see Figure 2b). This is given by

$$\phi_c = 180 - \omega_c \qquad (8)$$

where ω_c is the value of ω at the point $X = r_c$ obtained from the integration of the bubble surface.

The tangent to the surface of the meniscus at the point of contact makes an angle Ψ_c with the horizontal. This angle Ψ_c is dependent on the gravity or the buoyancy force, and its value is obtained by the method suggested by Kralchevsky et al.[11] The elevation of the point of contact above the flat surface of the solution, h_c (see Figure 2), can be calculated by (see eq 15 in ref 13)

$$h_c = r_c \sin\Psi_c \ln\frac{4}{\gamma_e(\Delta\rho g/\sigma)^{1/2} r_c(1 + \cos\Psi_c)} \qquad (9)$$

where $\gamma_e = 1.781\,072\,418$ is Euler's number. An error estimate of the above equation is provided by Kralchevsky et al.[11] Since we have two unknowns, h_c and Ψ_c, we need a second equation. This equation is provided by the one derived by Princen,[22] with a small modification, and it is an exact equation. It is obtained from the condition of constancy of pressure at all points of the horizontal planes situated in the bulk gas and liquid phases (see eq 13 in ref 13)

$$\sin\Psi_c = \frac{r_c}{R_b}\left[1 + \frac{\beta}{2R_b}(z_c - h_c)\right] - \sin\phi_c \qquad (10)$$

where z_c is the height of the point of contact from the bottom of the bubble. By use of an iteration procedure between these two equations, the values of h_c and Ψ_c are obtained.

iv. Theoretical Description of the Interference Pattern. From the profiles of the meniscus and bubble surfaces, it is possible to calculate the position at which interference fringes will occur. As we had already mentioned, the profile of the bubble surface is obtained by integrating the Laplace equations for the bubble. The profile of the meniscus can then be obtained by integrating the Laplace equations for the meniscus.[21] The equations are given by

$$\frac{d\sin\omega_m}{d\hat{x}} = \frac{-\sin\omega_m}{\hat{x}} - \hat{z}\beta$$

$$\frac{d\hat{z}}{d\hat{x}} = -\tan\omega_m \qquad (11)$$

where $\hat{x}$ and $\hat{z}$ are dimensionless as before and ω_m is the angle made with the normal to the surface and the vertical. The boundary conditions for the two surfaces are

$$X = r_c;\ \frac{d\hat{z}_b}{d\hat{x}} = \tan(180 - \phi_c) = \tan\omega_c;\ Z_b = h_c$$

for the bubble and

$$X = r_c;\ \frac{d\hat{z}_m}{d\hat{x}} = -\tan\Psi_c;\ Z_m = h_c$$

for the meniscus. The subscripts m and b refer to the meniscus and bubble surface.

Using the Runge–Kutta method, we integrated the two surfaces simultaneously, with respect to x. When the distance between the two surfaces ($Z_m - Z_b$) satisfies the condition for interference, i.e.

$$Z_m - Z_b = h_k = k\lambda/4N \quad (k = 1, 2, 3, ...) \qquad (12)$$

(where N is the refractive index of the solution and h_k is the distance which satisfies the condition for interference) the position of a theoretical fringe is obtained. The integration is carried out until the number of theoretical fringes obtained equals the number of experimental fringes observed.

In the case of two surfaces (in our case these are the meniscus and the bubble surface), the rays of light arriving vertically are deviated by refraction and reflection at the surfaces (see Figure 7). The corrected distance h_k is

(21) Hartland, S.; Hartley, R. In *Axisymmetric Fluid–Liquid Interfaces;* Elsevier Science: New York, 1976.
(22) Princen, H. M. *J. Colloid Interface Sci.* **1963**, *18*, 178.
(23) Nikolov, A. D.; Dimitrov, A. S.; Kralchevsky, P. A. *Opt. Acta* **1986**, *33*, 1359.
(24) Beyer, H. *Theorie und Praxis der Interferenz Mikroskopie*; Leipzig: Akademishe Verlagsgesellschaft Geest u. Portig, 1974.

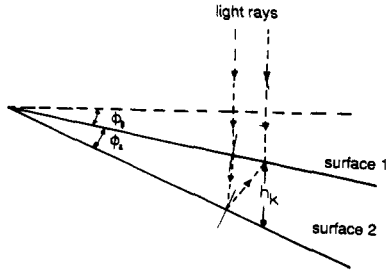

Figure 7. Reflection and refraction at an inclined wedge.

given by

$$h_k = \frac{\lambda}{4N}(k+1) \times \frac{2\cos^2(r+\phi_2)}{\cos(r+2\phi_2)\cos(\phi_1+\phi_2)[1+\cos(2r+\phi_2)]} \quad (13)$$

where ϕ_1 and ϕ_2 are the angles described in Figure 7. These angles are obtained from integration of the Laplace equation

$$\phi_1 = \omega_m; \quad \phi_2 = 180 - \omega_m - \omega_b$$

ω_m and ω_b are the angles of the Laplace equation for the meniscus and the bubble, respectively. These angles are updated at every integration step

$$r = \arcsin[(\sin\phi_1)/N]$$

where N is the refractive index of the solution. The cosine terms on the right correct for reflection and refraction at a wedge. The condition for the occurrence of the fringes is when the distance between the two surfaces ($Z_m - Z_b$) is equal to h_k, where h_k is given by eq 13.

v. Minimization of Dispersion between Experimental and Theoretical Radii. The disparity between the positions of theoretical and experimental rings is given by the dispersion

$$\mu(r_c) = \sum_{i=1}^{n}[r_e(i) - r_t(i)]^2 \quad (14)$$

where n is the number of rings observed in the experiments, $r_t(i)$ the radius of theoretical interference ring, and $r_e(i)$ the radius of experimental interference ring.

The ideal match for the experimental and theoretical results would result in the dispersion tending to zero. However, due to limitations in experimental accuracy, this ideal cannot be achieved. We obtain the best fit when the value of the dispersion is minimum. The match between the theoretical and experimental values of the radii of the rings depends on the initial value of r_c chosen in step ii. Hence, the dispersion is a function of r_c, and the value of r_c is varied in such a way as to minimize the dispersion. For every change in the value of r_c, the calculation steps i to v are repeated.

At the minimum dispersion, the contact angle α can be calculated (see Figure 2) by

$$\alpha = \phi_c - \Psi_c \quad (15)$$

Calculation of Angle θ Using the Differential Interference Fringes. From the force balance equations of a fluid particle at a fluid interface, Ivanov et al.[10] deduced that in the absence of line tension the condition for equilibrium of the particle requires that

$$\theta = \alpha/2 + \Psi_c \quad \text{(see Figure 2)} \quad (16)$$

From the streaks, the value of R_f can be calculated by using eq 1. From graphical interpolation, the values of R_f are obtained for the instants at which common interference measurements are available. From the value of r_c calculated from CI measurements and R_f calculated from DI measurements, the angle θ is obtained:[13]

$$\theta = \arcsin(r_c/R_f) \quad (17)$$

Hence independent measurements from the DI and CI patterns could be used to obtain the angles at the point of contact and to check the validity of eq 16 for the equilibrium of the particle. This check could be used in the case of larger bubbles, where line tension effects can be neglected.

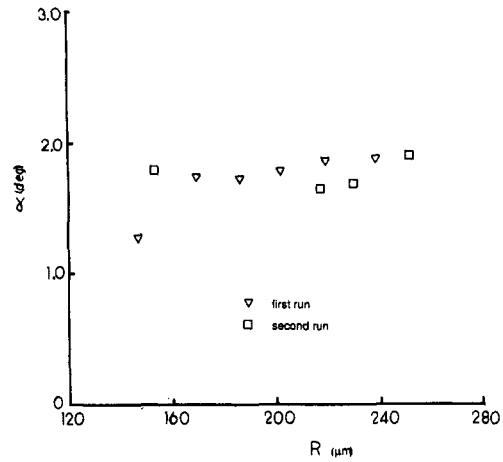

Figure 8. Contact angle as a function of the bubble radius obtained from two experiments made on the system containing 1 wt % AE 9.4.

Results and Discussions

To confirm that the experiments are reproducible, we measured two individual bubbles for the test solution containing 1 wt % surfactant with 1 wt % NaCl. The contact angle α, obtained by the minimization procedure, is plotted against R, for the two runs, in Figure 8, showing a reproducibility of 0.2°. Hence, if the experiments are performed in the manner described, reproducible results are obtainable.

Contact Angle from Common Interference Measurements. Using the radius of contact as the variable parameter, we minimized the dispersion, obtaining a good fit between the theoretically calculated and experimentally measured values of the radii of the Newton rings (see Figure 9). The standard deviation of the radii of the rings was 0.1 μm for both the systems, which is within the limits of experimental accuracy. Figure 10 shows the contact angle α as a function of the radius of the bubble obtained from the experiments. The plot of r_c versus the capillary pressure π (which is calculated from the radius of curvature of the bottom of the bubble) is shown in Figure 11.

From Figure 10, we see that for bubbles larger than 160-μm radius, the contact angle α is practically independent of the bubble size. This is confirmed by the results obtained from differential interference measurements and discussed in the next subsection. We also observed, for both systems, that the ratio of R to r_c decreased from 10.1 to 4.2 with a decrease in the bubble radii from 300 to 125 μm. This result indicates a large deformation of the lower bubble surface and the meniscus, near the three-phase contact line. This occurs because of the effect of gravity, because when the effect of gravity is negligible, r_c/R equals sin α (which is nearly constant in our case for $R > 160$ μm).

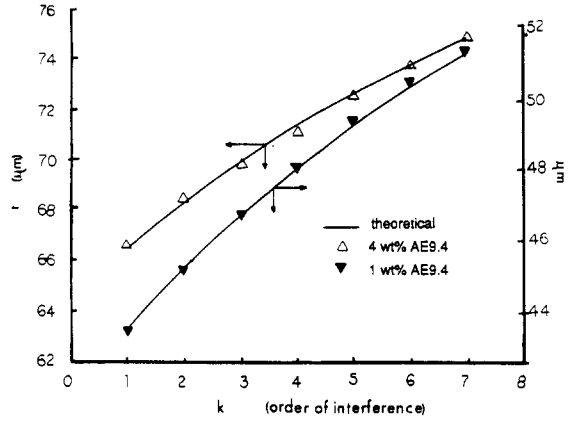

Figure 9. Best fit of the radii of the Newton rings between those obtained theoretically and those measured experimentally for bubbles of the two systems at their largest size (first measurements).

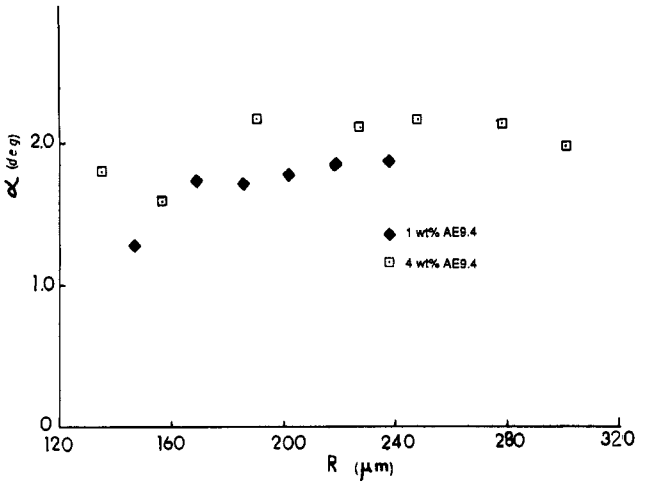

Figure 10. Contact angle as a function of the bubble radius for the two experimental systems.

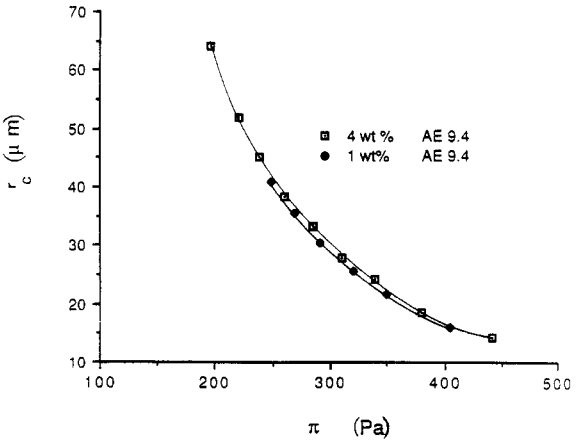

Figure 11. Radius of contact of the film, r_c, as a function of the capillary pressure.

Differential Interference Measurements. Measurements made by Nikolov et al.[23] on sessile liquid drops show that the correction for the aperture suggested by Beyer[24] is small and random. Hence, this correction is taken to be zero. Due to the diffuse nature of the streaks, as compared to the sharp streaks obtained by Nikolov et al.[12] using SDS, the experimental error in measuring R_f was about 4–5%. The plots of R versus R_f for the two systems are shown in Figure 12. From these plots, interpolated values of R_f were obtained to calculate values of

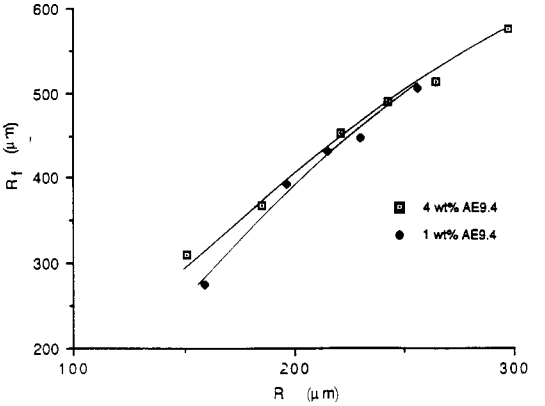

Figure 12. Radius of curvature of the film R_f as a function of the bubble radius R.

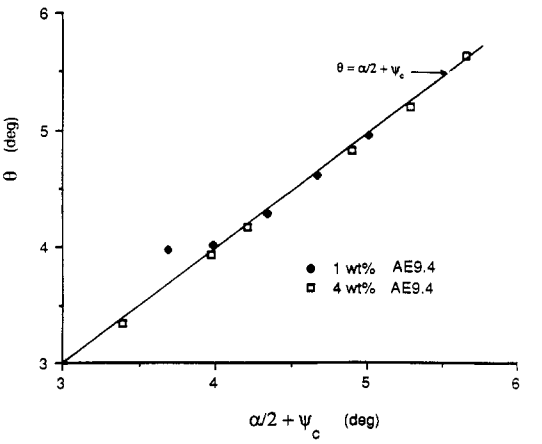

Figure 13. Plot of θ vs $\alpha/2 + \Psi_c$ for the two experimental systems.

θ which were then compared with the calculated values of α and Ψ_c from the common interference measurements, as explained before. Note that only interpolated values were used; if one requires extrapolated values, they must be used with caution.

The plot of θ versus $\alpha/2 + \Psi_c$ for the two systems is shown in Figure 13. The data lie close to the line $\alpha/2 + \Psi_c$ (the experimental accuracy of the measurements of the angle α is 0.15°). All the differential measurements were made for bubble radius $R > 160$ μm. Below this value, the splitting of the two images is almost complete, and the streaks do not exist. Hence, it was not possible to calculate R_f (unless extrapolation is used) for bubble radii lower than 160 μm. Study of smaller sized bubbles would necessitate the use of another objective with larger magnification.

The plots of θ versus $\alpha/2 + \Psi_c$ confirm that for bubbles larger than 160 μm the line tension can be neglected.[10] This agrees with the results obtained from the CI measurements—the contact angle α is independent of R for $R > 160$ μm. The small decrease in contact angle for smaller bubbles ($R < 160$ μm) may be due to the effect of appreciable line tension; pursuing that possibility, however, is not in the scope of this study.

Effect of Micellar Concentrations. In comparing the values of the contact angle α for the solutions of two different micellar concentrations, we observed an interesting effect: the contact angle decreases by about 0.35° with a decrease in surfactant concentration from 4 to 1 wt %. This phenomenon indicates a decrease in the film thickness with an increase in the contact angle. This effect could be caused by the osmotic pressure of the micelles. If it is assumed that there are no micelles in the film, the

osmotic pressure within the film increases with the micellar concentration in the bulk solution, resulting in a movement of the solution from within the film to the bulk. This would result in thinner films and larger contact angles for higher concentrations of the micellar phase.

In stratifying films it is also possible to reach a metastable state with micelles being present within the film.[16] In this case, the contact angle depends on the interaction between the micelles within the film. The size and the shape of the micelles, and hence the micellar interactions, are a function of the surfactant concentration. A variation in the micellar interactions (with concentration) within the surfactant film could result in a change in the contact angle that we observed.

Conclusions

The new method to measure contact angles of floating bubbles involved matching the values of the radii of the Newton rings generated by solving the Laplace equations for the various surfaces to those obtained from the experimental interference pattern. We obtained a good fit between the two with a standard deviation of 0.1 μm, which is within the limits of the accuracy of the experimental measurement. The method to determine the contact angle does not make use of any major assumption. Studies were made with an ethoxylated alcohol surfactant Enordet C1415 AE9.4 at concentrations of 1 and 4 wt %, which were several times the cmc of the surfactant. The values of the contact angle that we obtained for this system were as low as 2°. Two experiments were carried out with the solution containing 1 wt % surfactant to check the reproducibility. The experimental technique and the measurements were reproducible to within 0.2° for the contact angle.

The results obtained by using the new procedure show that the contact angle is independent of the capillary pressure for the larger bubbles ($R > 160$ μm). To confirm this, we measured the angles θ, α, and Ψ_c at the radius of contact using measurements made from the differential and common interference patterns. The values of these angles were used to check the validity of the equation of equilibrium of the particle (eq 16). The results show that for these larger bubbles line tension effects are negligible.

We observed a 0.35° increase in the value of the contact angle α in increasing the surfactant concentration from 1 to 4 wt %. This effect could be caused by osmotic pressure effects or the change in the interactions of the micelles within the film at higher micellar concentrations. We are making further studies to determine its cause.

Acknowledgment. This work was supported in part by the Department of Energy, the National Science Foundation, and the Bulgarian Ministry of Culture, Science and Education. We are grateful to Prof. I. B. Ivanov for his interest and useful suggestions.